fractal and fractional

MDPI

Article

Microgrid Frequency Regulation Based on a Fractional Order Cascade Controller

Soroush Oshnoei [1,2], Arman Fathollahi [1], Arman Oshnoei [3,*] and Mohammad Hassan Khooban [1]

[1] Department of Electrical and Computer Engineering, Aarhus University, 8000 Aarhus, Denmark
[2] Department of Electrical Engineering, Shahid Beheshti University, Tehran 1983969411, Iran
[3] Department of Energy (AAU Energy), Aalborg University, 9220 Aalborg, Denmark
* Correspondence: aros@energy.aau.dk

Abstract: Nowadays, the participation of renewable energy sources (RESs) and the integration of these sources with traditional power plants in microgrids (MGs) for providing demand-side power has rapidly grown. Although the presence of RESs in MGs reduces environmental problems, their high participation significantly affects the system's whole inertia and dynamic stability. This paper focuses on an islanded MG frequency regulation under the high participation of RESs. In this regard, a novel fractional order cascade controller (FOCC) is proposed as the secondary frequency controller. In the proposed FOCC controller structure, a fractional order proportional-integral controller is cascaded with a fractional order tilt-derivative controller. The proposed FOCC controller has a greater degree of freedom and adaptability than integer order controllers and improves the control system's efficiency. The adjustable coefficients of the proposed controller are tuned via the kidney-inspired algorithm. An energy storage system equipped with virtual inertia is also employed to improve the system inertia. The proposed FOCC controller efficiency is compared with proportional-integral-derivative (PID), tilt-integral-derivative (TID), and fractional order proportional-integral-derivative (FOPID) controllers under different disturbances and operating conditions. The results demonstrate that the presented controller provides better frequency responses compared to the other controllers. Moreover, the sensitivity analysis is performed to show the proposed controller robustness versus the parameters' changes in the system.

Keywords: islanded microgrid; frequency regulation; renewable energy sources; fractional order controllers; cascade controller

Citation: Oshnoei, S.; Fathollahi, A.; Oshnoei, A.; Khooban, M.H. Microgrid Frequency Regulation Based on a Fractional Order Cascade Controller. *Fractal Fract.* **2023**, *7*, 343. https://doi.org/10.3390/fractalfract7040343

Academic Editors: Costas Psychalinos and Da-Yan Liu

Received: 11 December 2022
Revised: 1 April 2023
Accepted: 18 April 2023
Published: 21 April 2023

1. Introduction

Assembling the highest usage of renewable energy sources (RESs) and distributed energy generators (DEGs) has become a worldwide consensus in recent years as the situation surrounding energy security, global warming, and environmental degradation has become more complex [1]. It is now impossible to imagine a future without new power systems that derive a significant portion of their electricity from large-scale RESs such as photovoltaic power plants (PPP) and wind power plants (WPP) [2–4]. In the last decade, the collection and integration of RESs and DEGs in microgrids (MGs) have played an essential role in providing power systems load [5]. Due to information provided by the International Renewable Energy Agency, the generation capacity of RESs across the world reached 2537 GW in recent years. The capacity of hydropower energy sources is estimated to be 1190 GW, assembling them the most extensive share of the global total. This was followed by wind, solar, bioenergy, geothermal, and marine energy resources with the capacity of 623 GW, 586 GW, 124 GW, and 14 GW, respectively. Note that marine energy accounted for the smallest share of the global total, with only 500 MW [6,7].

Traditional generators' frequency modulation capabilities are becoming inadequate as RESs become more integrated into power systems [8,9]. In addition, RESs [10] and energy storage systems (ESSs) [11] are widely used in MGs and power systems to decrease energy

consumption and enhance energy utilization efficiency. Although the presence of RESs in electricity grids significantly reduces the concerns related to environmental problems and the lack of fossil fuels, the intermittent nature of these sources affects the stability of grids [12,13]. Hence, ESSs are used in MGs due to the intermittent nature of output power in RESs [14]. Load frequency control (LFC) is a necessary service widely utilized in electricity grids to keep the system frequency in the acceptable range [15]. Since the LFC mechanism has an important impact on the electricity grid's stability, it is essential to study the frequency performance of these grids under the high penetration of RESs.

The MGs operate as part of the upstream utility grid when conditions are standard (grid-connected mode) but can switch to working independently if the utility grid encounters an outage or fault (standalone mode) [16]. One of the significant threats in standalone MGs operating conditions is the output powers of WPPs and PPPs due to the erratic behavior of solar irradiation and wind speed, respectively. These conditions often lead to a discrepancy between supply and demand in MGs [17,18]. As a result, inertia response and frequency regulation may be lost if RESs are widely deployed in MGs. Under these circumstances, even moderate fluctuations in MG frequency may have destructive effects [19]. Therefore, it appears critical to implement appropriate control strategies in isolated MGs to improve the system inertia and frequency regulation.

Numerous control procedures for MGs have been reported in the literature to deal with this challenge. A local controller independently operates local control loops of each distributed generation in an MG at the primary level of hierarchical control [20,21]; the secondary level of control compensates for frequency and voltage changes generated by the primary level of control. Considering its efficiency and comfort of implementation, distributed secondary control has recently gained extensive attention [22]. Moreover, a methodology known as virtual inertia (VI) emulation has been developed to increase the rotational inertia of the MG. Emulating a VI with the help of the derivative technique is one of the more productive manners to go about it [23–25]. In recent years, researchers have been looking into how applying VI in islanded MGs could help improve the MG inertia response and frequency stability [12,26–28].

Nowadays, various control strategies, such as adaptive control [29], fractional order (FO) and integer-order (IO) controllers [16,21,30,31], cascade controllers [32–34], fuzzy-logic techniques [35,36], and H_∞ control theory [37], have been developed in the current works to improve the frequency response of MGs. Robust controller-based linear matrix inequality of an MG with different energy sources is reported in [38]. Ref. [39] proposes a robust control strategy to attain voltage and frequency stability. MG's closed-loop state-space model is elicited after creating a small-signal structure for a single distributed generation unit. The robust stability of the MG is then analyzed using a new Lyapunov–Krasovskii functional. Authors in [40] present a proportional-integral-double derivative controller as the secondary controller of an islanded MG to improve the system frequency regulation. An event-triggered controller regarding input delay and cyber-attack disturbances is proposed in [41] as the secondary frequency controller in an islanded MG. The authors in [42] propose an innovative fuzzy adaptive differential evolution algorithm for modifying a fuzzy logic-based controller to enhance the inertia control in MGs. In [19], the deep deterministic policy gradient is presented as a secondary controller of an island MG. To maintain voltage and frequency stability, the presented controller regulates the power delivered by the storage components. Several analyses employ progressive controlling techniques employing cascaded controllers [43,44] for the improved frequency control process of MGs.

In recent years, the development of science in engineering fields has greatly led to using fractional calculus in control applications. The leading cause for utilizing the IO models was the lack of suitable solution approaches for FO differential equations. FO controllers are dynamic systems modeled by FO differential equations. Numerous physical systems are not modeled with integer-order calculus. This is because their real dynamics include non-integer derivatives. Hence, FO calculus has been introduced to describe

such systems precisely. Conventional and IO controllers such as I, PI, and PID are not persistent versus changes in the system coefficients and operating conditions, which causes their performance to be significant. This is a notable flaw of such controllers [16]. In this regard, FO controllers, the FO version of the IO controllers, are introduced to address this problem [31]. The FO controllers have more degrees of freedom and flexibility compared to the IO controllers. In [31], the authors have proposed the hybrid controller—a combination of the tilt-integral-derivative (TID) and FO proportional-integral-derivative (FOPID)—to control the gate-controlled series capacitor installed in the tie-line of a multi-area power grid to enhance the system frequency response. A hybrid controller based on a two-degree-of-freedom design is proposed in [16] as the secondary controller to enhance the frequency stability of a two-area power grid. The authors in [45] have proposed a TID controller for frequency regulation of a power system integrated with WPP. In [46], a secondary PI controller is used to improve the frequency performance of a low-inertia power system in the presence of high penetration of electric vehicles. The authors have not presented any solutions to enhance the system inertia. A FO integral controller has been used in [47] to enhance the frequency stability of an interconnected MG considering the VI equipment. The authors in [48] have proposed a FO controller as the secondary frequency controller of a shipboard MG. In [49], a high-dimensional multiple FO controller has been presented to improve the frequency response of a two-area power system.

The fundamental problem with IO controllers is that constant parameters and no explicit details of the overall procedure and performance are compromised. Additionally, these controllers are linear and exhibit symmetry in special cases. Hence, their performance in nonlinear systems is unstable. Hence, such controllers require to be modified for process control applications. FO derivative is a convolution in FO differential equations. Therefore, it accurately describes the dynamics of inheriting memory and congenital features where IO derivative methods seem to fail. From the control perspective, fractional calculus permits the combination of further degrees of freedom in the control strategies, which can consider more effective limitations when designing the control rules. Fractional calculus can provide appropriate tools when IO calculus fails to perform satisfactorily regarding the design consideration involved. Furthermore, an FO controller is more flexible with a determined complexity growth. Consequently, investigating the control applications according to FO operators can have significant theoretical importance and overall possible significance in addressing the gap between theory and practice.

In addition to changes in the system coefficients and operating conditions, the traditional controllers' effectiveness in today's electricity grids significantly reduces due to the increasing complexities of these grids. To solve this, the cascade controller is introduced as a suitable candidate to improve system control performance. The cascade control concept comes from the control of two sequential procedures, where the inner procedure or output of the first supplies the second or outer procedure in sequence. The rationale behind this configuration is that the fast dynamics of the inner loop enable quick mitigation of perturbation and minimize the possible effects of perturbations before they impact the primary output. Accordingly, cascade controllers are employed in multi-loop control systems to quickly reject disturbance requirements and provide decent set-point tracking [32,33]. In [32], a cascade controller based on the FO and IO controllers is used as the secondary controller of a two-area MG to regulate the system frequency. Ref. [33] has proposed a cascade FO fuzzy PID-IDD controller for effective efficiency of tidal turbines in the LFC task of an island MG. The authors in [50] have proposed a cascade FOPD-PI controller for frequency regulation of an islanded MG without considering VI service. Ref. [51] has studied the LFC issue of a multi-area power system under communication delay and system physical limitations. In this regard, a FOPID controller cascaded with a first-order filter has been presented as the secondary controller.

According to the mentioned explanations, the design of a novel controller based on the FO and cascade controllers (FOCCs) aids in improving the system frequency performance, which is crucial in the hybrid deregulated energy system of MGs. Consequently, the

authors are motivated to propose a novel FOCC controller as the secondary controller in an islanded MG. Moreover, a kidney-inspired algorithm (KA) is employed for tuning the optimal coefficients of the suggested controller. Furthermore, to enhance the grid inertia and improve the frequency control problem of the system integrated with RESs, an ESS equipped with VI in coordination with the secondary controller is employed.

The contributions of this study are summarized as: (i) A novel FOCC controller is proposed as the secondary controller in the LFC problem of an islanded MG. In the proposed FOCC controller, FOPI controller is cascaded with a FOTD controller (ii). An ESS equipped with the VI is employed in the studied MG to enhance the total inertia of the system. (iii) The proposed control scheme's dynamic efficiency is compared with PID and TID controllers under various scenarios. (iv) The KA method is employed for optimizing the adjustable coefficients of the presented controllers. (v) The sensitivity analysis is conducted to investigate the presented controller's performance under the changes in the MG system parameters.

The current work is structured as follows: In Section 2, the studied MG modeling is described. Section 3 presents the design of the proposed FOCC controller. In Section 4, the KA optimization method is studied to tune the controller's parameters. The simulation results are illustrated in Section 5. Eventually, the conclusion of this work is provided in Section 6.

2. Microgrid Modeling

This section describes the studied MG modeling. Figure 1 demonstrates the simplified structure of the investigated MG. As illustrated, the MG comprises the different generation units such as a thermal power plant (TPP) with 12 MW, an ESS equipped with the VI with 4 MW, a WPP with 7 MW, and a PPP with 4 MW along with industrial and residential loads with 10 MW and 5 MW, respectively [25]. When a power imbalance occurs between generation power and load, the TPP and ESS receive the frequency deviation signal from the control center and participate in the frequency control problem of the system. Since WPP and PPP do not receive the frequency deviation signal, the output power of these units, together with load changes, are regarded as system disturbances.

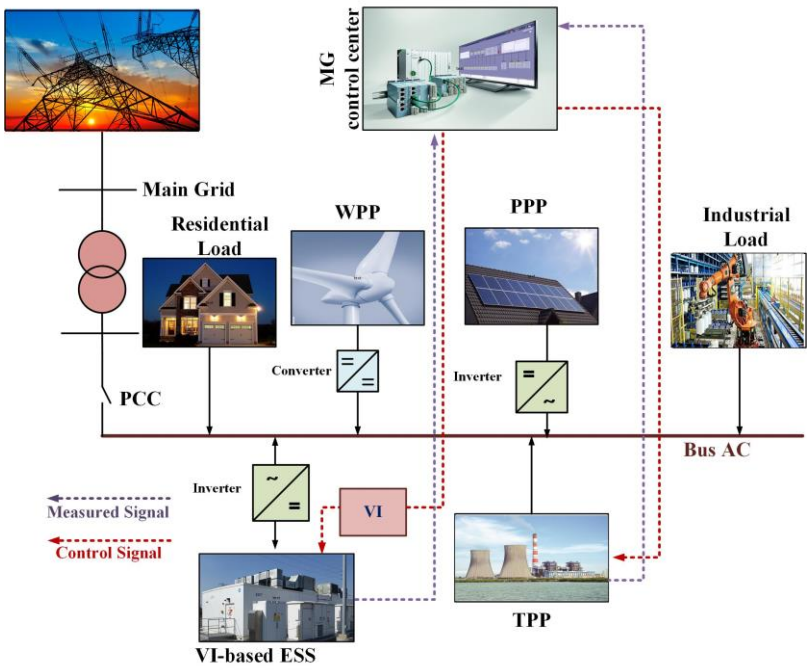

Figure 1. Schematic of the studied MG.

The LFC model of the islanded MG is represented in Figure 2. According to this figure, the TPP unit is composed of a governor, a non-reheat turbine, and a secondary frequency controller. Moreover, the non-linear limitations, such as generation rate constraint (GRC) and governor dead-band (GDB), are also employed in modeling the TPP to attain the real dynamic characteristics of the system. Therefore, the TPP output is restrained by the governor's valve position of 0.002 p.u.MW/s GDB and generator mechanical output of ±0.5 p.u. MW GRC for both rising and dropping rates. The modeling of the WPP and PPP generation resources is also performed using a first-order transfer function. In this study, a fractional order cascade controller is presented as the secondary frequency controller. The MG frequency deviation considering the generator inertia constant (H) and load damping coefficient (D) is written as follows:

$$\Delta f = \frac{1}{2Hs + D}[\Delta P_{TPP} + \Delta P_{VI} + \Delta P_{WPP} + \Delta P_{PPP} - \Delta P_{Load}] \quad (1)$$

where:

$$\Delta P_{TPP} = \left(\frac{1}{T_t s + 1}\right)\left(\frac{1}{T_g s + 1}\right)\left(\frac{1}{R}\Delta f - \Delta P_{ACE}\right) \quad (2)$$

$$\Delta P_{WPP} = \frac{K_{WPP}}{T_{WPP} s + 1}\Delta P_{wind} \quad (3)$$

$$\Delta P_{PPP} = \frac{K_{PPP}}{T_{PPP} s + 1}\Delta P_{solar} \quad (4)$$

where Δf is the MG frequency deviation, ΔP_{TPP}, ΔP_{VI}, ΔP_{WPP}, and ΔP_{PPP} denote the power changes in TPP, VI-based ESS, WPP, and PPP, respectively; ΔP_{wind} and ΔP_{solar} are the power variations in wind and solar irradiation, respectively; ΔP_{ACE} shows the secondary controller output, and finally, ΔP_{Load} expresses the power changes in the industrial and residential loads.

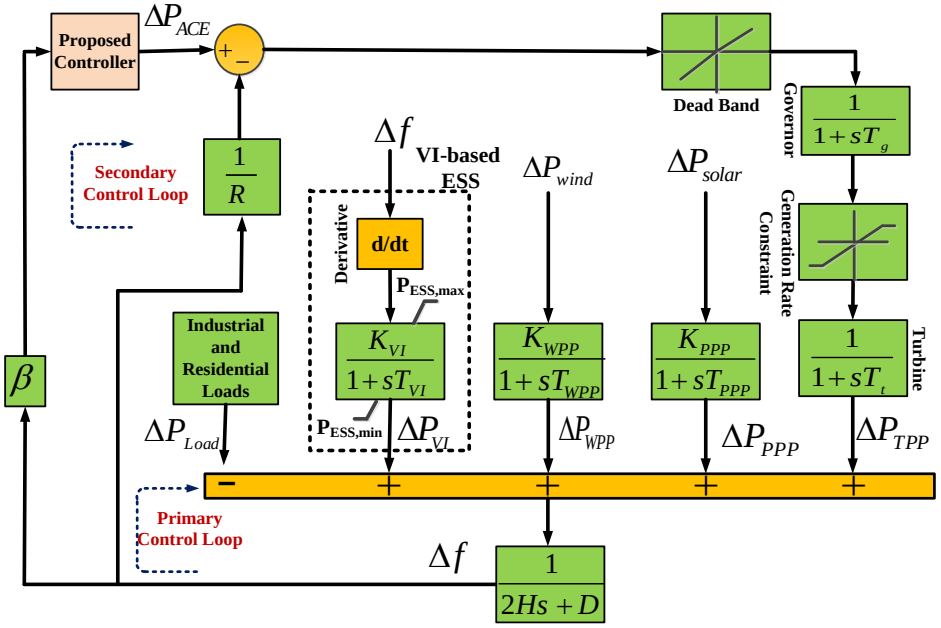

Figure 2. Diagram block of the islanded MG system.

VI is an effective tool to imitate the inertia features of the synchronous generator and enhance the MG frequency stability in the presence of high RESs contribution. The idea of VI is the derivative control that computes the rate-of-change of frequency to regulate the active power to the set point of the MG after the perturbations. In this work, the derivative technique is utilized to emulate the VI concept in the ESS [25]. The VI-based

ESS improves the whole inertia of the system. In addition to the derivative method, a first-order transfer function is also used to imitate the actual dynamic characteristics of the ESS, as demonstrated in Figure 2. Hence, the VI-based ESS can be controlled to provide the necessary active power to the system for enhancing the MG frequency performance. The VI power provided by the ESS ΔP_{VI} is expressed as:

$$\Delta P_{VI} = \frac{K_{ESS}}{T_{ESS}s + 1}\left(\frac{d}{dt}\Delta f\right) \tag{5}$$

Table 1 demonstrates the values and description of the parameters related to the investigated MG [26].

Table 1. Description and values of the MG parameters.

Parameter	Description	Value
H	System inertia (p.u.MW/s)	0.083
D	Load damping coefficient (p.u.MW/Hz)	0.015
T_g	Governor time constant (s)	0.1
T_t	Turbine time constant (s)	0.4
R	Governor droop constant (Hz/p.u.MW)	2.4
B	Frequency bias factor (p.u.MW/Hz)	1
K_{ESS}	ESS gain	0.8
T_{ESS}	ESS time constant (s)	10
K_{WPP}	WPP gain	1
T_{WPP}	WPP time constant (s)	1.5
K_{PPP}	PPP gain	1
T_{PPP}	PPP time constant (s)	1.85

3. Design of the Proposed Fractional Order Cascade Controller

This section describes the design of the presented fractional order cascade controller for the secondary controller to enhance the system's frequency regulation. The idea of the fractional calculus-based cascade controller is known as the FOCC. FO controllers are the FO version of the classical IO controllers [52–54]. These controllers have a greater degree of adaptability and flexibility than IO controllers. They can improve the FO controllers' performance in dealing with oscillations' amplitude and settling time in comparison to the IO controllers. IO controllers are extended to FO controllers utilizing fractional calculus. The generally utilized definitions for fractional derivative and integral are by Riemann–Liouville definitions [30,31] and are expressed by Equations (6) and (7), respectively:

$${}_aD_t^{\alpha} f(t) = \frac{1}{\Gamma(n-\alpha)}\frac{d^n}{dt^n}\int_a^t (t-\tau)^{n-\alpha-1} f(\tau)d\tau \tag{6}$$

$${}_aD_t^{-\alpha} f(t) = \frac{1}{\Gamma(\alpha)}\int_a^t (t-\tau)^{\alpha-1} f(\tau)d\tau \tag{7}$$

where $n-1 \leq \alpha < n$, n is an integer, $\Gamma(\cdot)$ shows the Euler's gamma function, and ${}_aD_t^{\alpha} f(t)$ denotes the fractional operator. Laplace's transformation of Equation (6) considering zero initial condition is represented as follows:

$$L\{{}_aD_t^{\alpha} f(t)\} = s^{\alpha}F(s) - \sum_{k=0}^{n-1} s^k {}_aD_t^{\alpha-k-1} f(t)|_{t=0} \tag{8}$$

for $n-1 \leq \alpha \leq n$, where $F(s) = L\{f(t)\}$ indicates Laplace's transformation. This paper employs the commande robust d'ordre non-entier (CRONE) approximation, presented by Oustaloup, out of several other approximations [16,21]. CRONE utilizes a recursive distribution of N poles and N zeros, conducting a transfer function during the predefined

frequency range $[\omega_l, \omega_h]$ [55–57]. In the simulation process, ω_l = 0.01 rad/s, ω_h = 100 rad/s, and N = 5 are presumed.

$$H_f(s) = s^{\alpha} = K \prod_{n=1}^{N} \frac{1 + (s/\omega_{z,\ n})}{1 + (s/\omega_{p,\ n})} \tag{9}$$

where K shows the tunable gain, $\omega_{z,\ n}$ and $\omega_{p,\ n}$ represent the zeroes and poles of $H_f(s)$, which are computed by (10)–(14).

$$\omega_{z,l} = \omega_l \sqrt{n} \tag{10}$$

$$\omega_{p,n} = \omega_{z,n} \tau, \qquad n = 1, \ldots, \ l \tag{11}$$

$$\omega_{z,n+1} = \omega_{p,n} \sqrt{n}, \qquad n = 1, \ldots, \ l-1 \tag{12}$$

$$\tau = (\omega_h / \omega_l)^{\varepsilon / N} \tag{13}$$

$$\sigma = (\omega_n / \omega_l)^{(1-\varepsilon)/N} \tag{14}$$

FOPID and TID controllers are the two well-known FO controllers. Typically, the transfer functions of these controllers are given by (15) and (16), respectively [31].

$$H_{FOPID}(s) = K_P + \frac{K_I}{s^{\lambda}} + K_D s^{\mu} \tag{15}$$

$$H_{TID}(s) = K_T s^{(-1/n)} + \frac{K_I}{s} + K_D s \tag{16}$$

where K_I, K_P, K_D, and K_T show the tunable integral, proportional, derivative, and tilt coefficients, respectively. λ and μ are the FO operators of the integral and derivative terms in the FOPID controller, respectively. n indicates the FO operator of the tilt term in the TID controller. λ and μ are adjusted in the range of (0, 1), and n is selected in (2, 3). Similar to controllers FOPID and TID, the transfer functions of the FOPI and FOTD or TD$^{\mu}$ controllers are expressed as:

$$H_{FOPI}(s) = K_P + \frac{K_I}{s^{\lambda}} \tag{17}$$

$$H_{TD}(s) = K_T s^{(-1/n)} + K_D s^{\mu} \tag{18}$$

FO controllers are the appropriate candidates to control the system dynamic; accordingly, cascading the FO controllers can significantly improve the system's dynamic efficiency. In this study, cascading the FOPI and TD$^{\mu}$ controllers is proposed as the secondary frequency controller.

The control of two successive processes relates to the idea of cascade control. Cascade control can increase the efficiency of the control system in comparison to single-loop control [33]. Figure 3 demonstrates the structure of the cascade control system. As shown, the cascade control includes two inner and outer control loops, in which the inner loop output provides the second process or input of the outer loop. The inner loop in the cascade control, known as the slave controller, rejects the effects of perturbations in a comparatively quicker procedure before transferring them to different parts of the plant. The inner loop mainly alleviates the impact of deviations related to the internal process coefficients (owing to set-point variations and perturbations) on the control system's efficiency. The outer loop, known as a master controller, handles the final output quality of the process to attain a reference signal $R(s)$ [34].

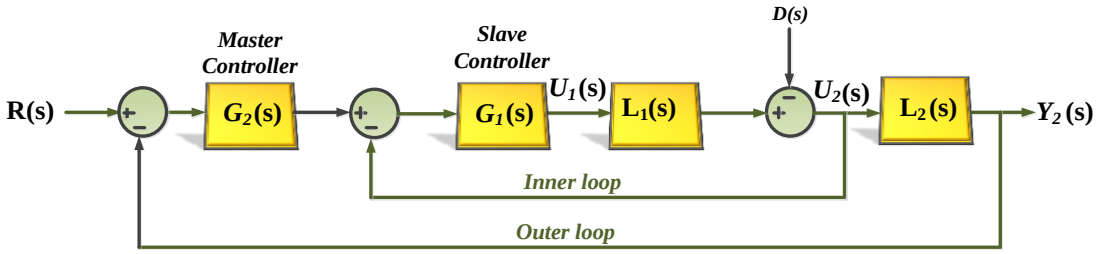

Figure 3. Structure of the cascade controller.

According to Figure 3, $G_1(s)$ and $G_2(s)$ indicate the transfer functions relevant to the slave and master controllers, respectively [58]. Moreover, $L_1(s)$ and $L_2(s)$ are the transfer functions associated with plants of the inner and outer loop, respectively. The system's final output $Y_2(s)$ subjected to load disturbance $D(s)$ is given by (19):

$$Y_2(s) = U_2(s)L_2(s) + D(s) \tag{19}$$

where $U_2(s)$ is the inner loop output or outer loop input. $U_2(s)$ controls $Y(s)$ signal to track $R(s)$. Likewise, the inner loop output $Y_1(s)$ can be obtained as:

$$Y_1(s) = U_2(s) = U_1(s)L_1(s) \tag{20}$$

The proposed control system in this study combines the FOPI&TD$^{\mu}$ controllers to construct a cascaded system. FOPI controller is cascaded with TD$^{\mu}$ controller, where FOPI controller forms the master controller $G_2(s)$ and TD$^{\mu}$ controller the slave one $G_1(s)$.

$$G_2(s) = K_P + \frac{K_I}{s^{\lambda}} \tag{21}$$

$$G_1(s) = K_T s^{(-1/n)} + K_D s^{\mu} \tag{22}$$

Consequently, the closed loop transfer function of the cascaded system is represented as follows:

$$Y_2(s) = \left[\frac{L_2(s)L_1(s)G_2(s)G_1(s)}{1 + G_1(s)L_1(s) + L_2(s)L_1(s)G_2(s)G_1(s)}\right]R(s) + \left[\frac{L_2(s)}{1 + G_1(s)L_1(s) + L_2(s)L_1(s)G_2(s)G_1(s)}\right]D(s) \tag{23}$$

Figure 4 illustrates the block diagram of the proposed FOPI and TD$^{\mu}$ cascade controller. To design the proposed FOCC, the adjustable parameters of the FOPI and TD$^{\mu}$ controllers are tuned by the KA method.

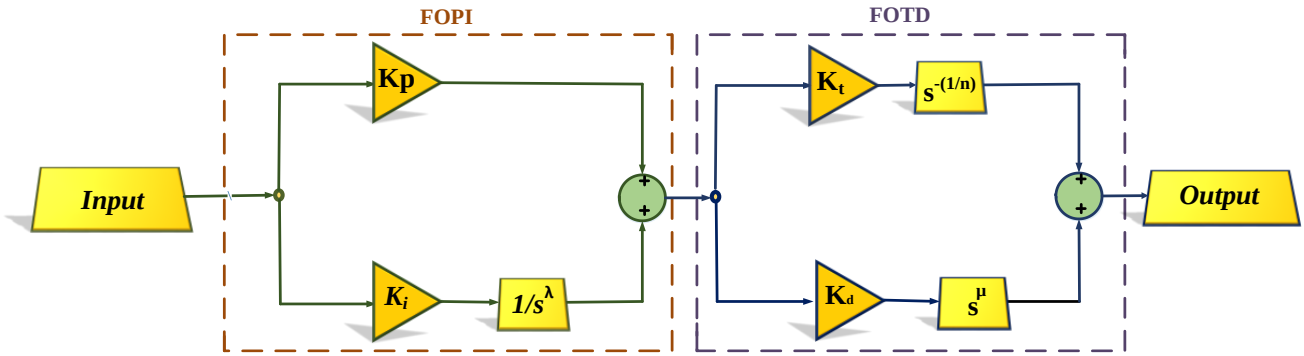

Figure 4. Diagram block of the proposed controller.

4. Optimization Algorithm to Tune the Controller's Coefficients

A new kidney plays a crucial role in the human body by filtering the blood, getting rid of extra fluid and toxins in the form of urine, and regulating the levels of ions in the blood. Since they regulate these processes, they are ultimately in charge of the human body's health. A superior optimization strategy called the KA was invented by exploring and utilizing the features of the human kidney's operating system [59]. In this section, the KA is employed for adjusting the parameters of the suggested FOPI&TD$^{\mu}$ cascade controller. The four primary components of renal treatments that are mentioned in the imitation are as follows: (1) transferring solutes and water from the blood to the tubules, referred to as filtration; (2) transporting important water and solutes from the tubules to the circulation, referred to as reabsorption; (3) transferring more harmful substances from the circulation to the tubule, known as secretion; and (4) transmitting the toxic substances from the first process stages into the urine, which is called excretion.

A total population of potential solutes is formed based on the real mechanism of kidneys in the KA's first stage. Their goal functions are computed in the same way as in other population-based computational methods. In the biological renal system, each solute can be thought of as water particles and solutes in plasma [60]. By gradually improving upon the best solute found so far, a new solute is generated for all solutes at the end of each cycle. In this algorithm, solute motion is defined as:

$$So_{j+1} = rand\ (So_{best} - So_j) + So_j \tag{24}$$

where S denotes a sample solution from the population. At iteration j the answer is So_j. So_{best} is the best solution found by the KA method in prior iterations, while $rand\ (So_{best} - So_j)$ is a random number between zero and the provided number.

The filtration operation separates the population's higher-quality solutes into filtered blood (FB), whereas the lower-quality solutes are flushed down the waste (W). A filtering rate is employed in the KA for this purpose and is computed and updated with each iteration. In a way similar to the manner the glomerular filtration rate is determined in a living kidney, the following equations specify the filtration rate (FR) [60,61]:

$$FR = \partial \times \sum_{j}^{n} f(y_j)/n \tag{25}$$

In this equation, $f(y_j)$ is the objective function of solution y at iteration j, n is the population size, and ∂ is a constant in the interval (0, 1].

In the KA algorithm, if the solute's quality is better than FR, then it is identified as a member of FB, and if it is lower than FR, then it is taken as a member of W. Solutes that are initially excluded from FB due to the reabsorption operator are given another opportunity to meet the quality criteria for inclusion. This is possible only if, after applying the motion operator in Equation (24) once more, the filtration rate is satisfied. This is analogous to how the kidneys of a living organism recycle healthy molecules back into the bloodstream. If this probability is not satisfied, the solute is extracted from W and substituted by a different solute. Further, the worst solute in FB is secreted (removed) if a solute put to FB is better than the worst in FB after the filtration operation. A solute is secreted if it is not preferable to the worst solute in FB. It is similar to how the kidneys filter dangerous substances out of the blood. The solutes in FB are then ranked so that the best one can be updated [61].

Last but not least, a new population is assembled by merging FB and W, and the filtration rate is consequently modified. This cycle of repetition stops once the termination condition is met. The continuous influx of water and solutes into a biological kidney system's glomerular capillary can be analogized to adding random solutes. The procedure code of the KA algorithm is illustrated in Algorithm 1 [60].

To evaluate the effectiveness of the suggested FOPI&TD$^{\mu}$ cascade controller, it is essential to define a proper objective function. In this regard, this paper considers the integral of time absolute error (ITAE) as a constrained optimization problem:

Objective Function:

$$Min \qquad ITAE = \int_0^{T_{sim}} t.|\Delta f|.dt \tag{26}$$

Decision Variables:

$$K_P,\ K_I,\ K_T,\ K_D,\ \lambda,\ \mu,\ n \tag{27}$$

Subject to:

$$\begin{gathered} K_{P_{min}} \le K_P \le K_{P_{max}},\ K_{I_{min}} \le K_I \le K_{I_{max}},\ K_{D_{min}} \le K_D \le K_{D_{max}} \\ K_{T_{min}} \le K_T \le K_{T_{max}},\ 0 \le \lambda,\ \ \mu \le 1,\ \ 2 \le n \le 3 \end{gathered} \tag{28}$$

Algorithm 1. The pseudo-code of the KA algorithm

I: set the population
II: evaluate the solute in the papulation
III: set the best solute (So_{best})
IV: set filtration rate (FR, Equation (25))
V: set waste (W)
VI: set filtered blood (FB)
VII: set number of iteration (numofiter)
VIII: ***while*** *(iter < numofiter)* ***do***
IX: ***for*** *all* So_j
X: generate new So_j *(Equation (24))*
XI: check the So_j *using FR*
XII: ***if*** So_j *assigned to W*
XIV: apply reabsorption and generate So_{new} *(Equation (24))*
XVI: ***if*** *reabsorption is not satisfied (*So_{new} *cannot be a part of FB)*
XV: remove So_j *from W (excretion)*
XVII: insert a random S into W to replace So_j
XVIII: ***end if***
XIX: So_{new} *is reabsorbed*
XX: ***else***
XXI: ***if*** *it is better than the* So_{worst} *in FB*
XXII: So_{worst} *is secreted*
XXIII: ***else***
XXIV: So_j *is secreted*
XXV: ***end if***
XXIV: ***end if***
XXV: ***end for***
XXVI: rank the S from FB and update the So_{best}
XXVII: merge W and FB
XXVIII: update filtration rate (Equation (25))
XXIX: ***end while***
XXX: return So_{best}

In the considered objective function, the settling time and the fluctuations' amplitude are the criteria that should be improved. The advantages of the ITAE index compared to the integral of absolute error (IAE) and integral of square error (ISE) indices have been presented in [62–64]. Table 2 illustrates the optimal values of the controllers' parameters via the KA method.

Table 2. Optimal values of the controllers' parameters using the KA algorithm.

Controller	K_P	K_I	K_D	K_T	λ	μ	n
PID	0.5	−1.2	0.5	-	-	-	-
TID	-	−1.34	0.67	0.74	-	-	3
FOPID	0.95	−1.75	0.75	-	0.5	0.3	-
Proposed FOCC	−9.5	5.8	0.9	0.5	0.1	0.4	3

5. Simulation Results

This section provides the simulation outcomes of the MG system designed in Section 2 employing the proposed FOCC controller as the secondary controller. The PID, TID, and FOPID controllers are also considered as other comparative control methods to study the effectiveness of the suggested FOCC controller. The presented controller performance is studied under various patterns of solar irradiation, wind speed, and load perturbations. Moreover, the sensitivity analysis is performed to evaluate the presented controller performance against the system's parameter changes. The simulations are accomplished on a system with Intel core 7i, CPU of 2.7 GHz, and 64-bit processor using MATLAB/SIMULINK (R2021b) software.

5.1. Scenario 1

In this scenario, a step industrial load change of 0.15 p.u.MW and a step residential load change of 0.1 p.u.MW are applied to the system at times = 15 and 80 s, respectively, as illustrated in Figure 5a. The patterns of the solar irradiation and wind speed changes are depicted in Figure 5b,c, respectively. The system frequency response related to this scenario is shown in Figure 5d. Concerning this figure, it can be said that the proposed controller presents a better frequency performance from the viewpoints of the lower fluctuations' amplitude and shorter settling time than the other controllers. The performance criteria of the ITAE and ISE related to the considered controllers are demonstrated in Table 3. As indicated, the proposed controller provides the lowest ITAE and ISE values than the other controllers. In addition, Table 4 indicates the mean absolute MG frequency deviation (MAGFD) employing the considered controllers for scenario 1. As depicted, the suggested controller prepares the lowest value compared to other controllers indicating its better efficiency in mitigating the oscillations.

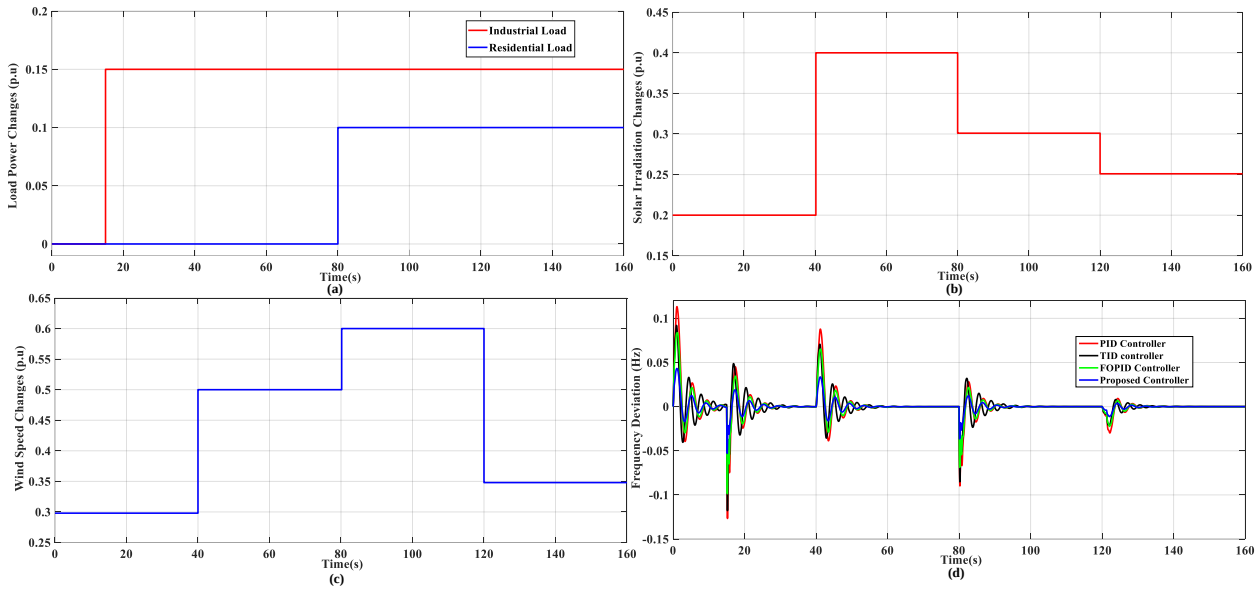

Figure 5. Perturbations and simulation result for scenario 1. (**a**) Load disturbances. (**b**) Wind speed changes. (**c**) Solar irradiation changes. (**d**) Obtained frequency responses.

Table 3. ITAE and ISE performance criteria of the MG frequency deviation employing different controllers.

Index	PID	TID	FOPID	Proposed FOCC
ISE	0.0464	0.0352	0.0285	0.0111
ITAE	0.597	0.472	0.349	0.194

Table 4. Evaluation index of the MG frequency deviation employing different controllers.

	PID	TID	FOPID	Proposed FOCC
Scenario 1	0.0103	0.0097	0.0081	0.005
Scenario 2	0.0541	0.05	0.0425	0.0273
Scenario 3	0.0421	0.038	0.0322	0.0207
Scenario 4	0.0386	0.0348	0.0291	0.0183
Scenario 5	0.0321	0.0283	0.025	0.0152

5.2. Scenario 2

This scenario considers the sequence of step load changes as the load disturbances and random changes for the solar irradiation and wind speed to evaluate the proposed FOCC performance. Figure 6 a–c depicts changes relevant to solar irradiation, wind speed, and load, respectively. The MG frequency response obtained by the presented controllers is shown in Figure 6d. This figure clearly shows that the presented controller provides a better frequency response against the designed disturbances compared to the others. The MAGFD attained by the presented controllers for this scenario is disclosed in Table 4. Clearly, the presented FOCC controller has the lowest value among the controllers and presents a more suitable frequency response than the other controllers.

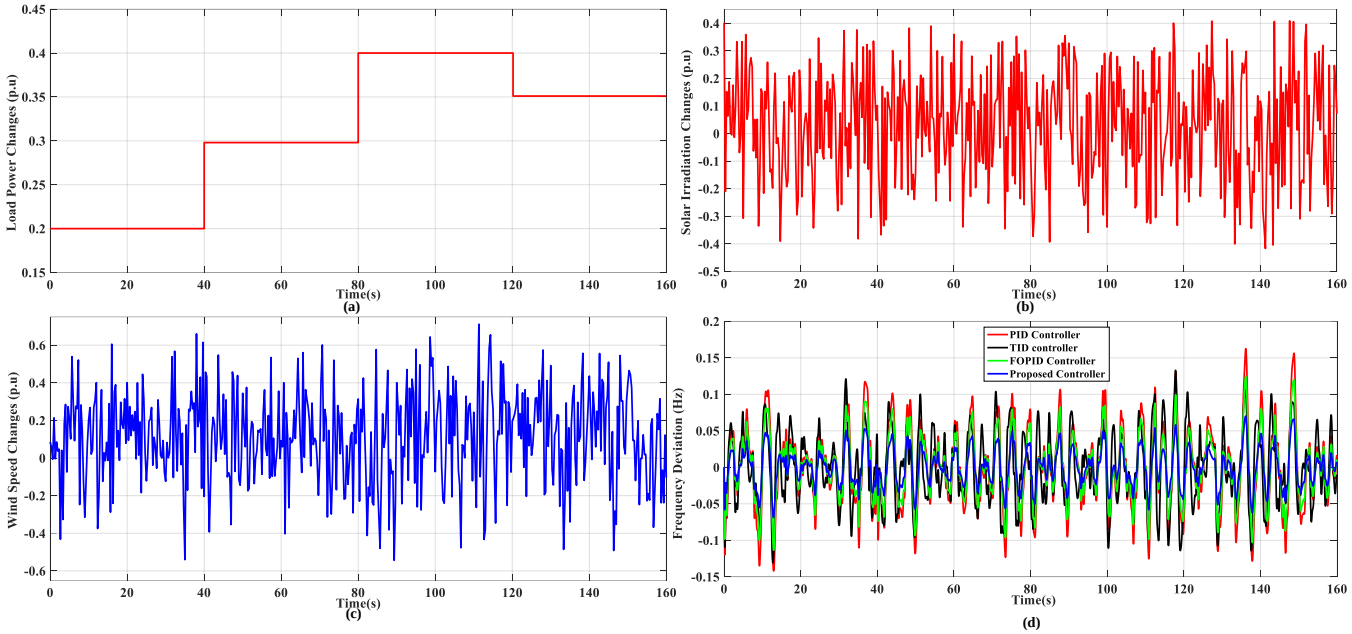

Figure 6. Perturbations and simulation result for scenario 2. (**a**) Load disturbances. (**b**) Wind speed changes. (**c**) Solar irradiation changes. (**d**) Obtained frequency responses.

5.3. Scenario 3

In this scenario, the suggested controller efficiency is investigated under random residential and industrial changes, as shown in Figure 7a. Patterns associated with solar

irradiation and wind speed disturbances are presented in Figure 7b,c, respectively. It is evident that the presented FOCC controller provides better handling of the disturbances and improves the system's dynamic performance compared to other controllers. Table 4 indicates the MAGFDs of this scenario. The proposed controller in this scenario has the lowest MAGFD compared to the other controllers, as in the prior scenarios.

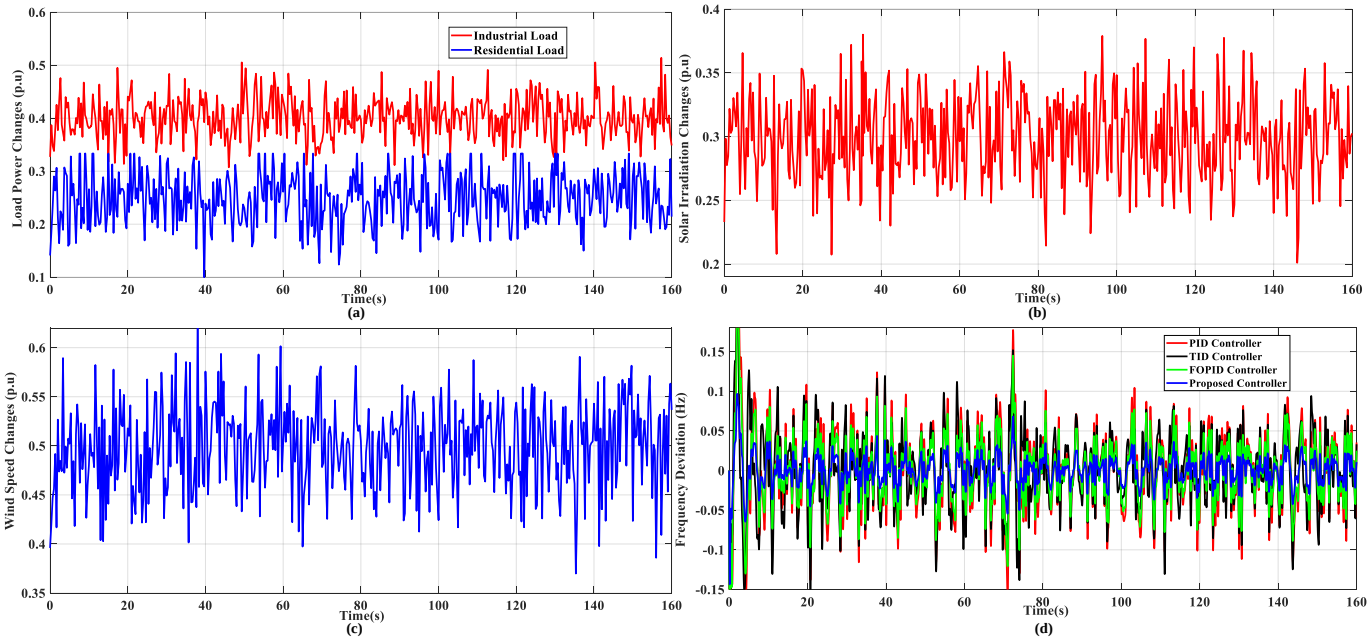

Figure 7. Perturbations and simulation result for scenario 3. (**a**) Load disturbances. (**b**) Wind speed changes. (**c**) Solar irradiation changes. (**d**) Obtained frequency responses.

5.4. Scenario 4

This scenario studies the proposed FOCC efficiency under a 30% reduction in the K_{ESS} value. Figure 8a–c depicts the random perturbations of the loads, solar irradiation, and wind speed, respectively. Figure 8d illustrates the MG frequency response employing the considered controllers. It can be seen that the fluctuations' amplitude is remarkably diminished using the proposed FOCC controller than the other controllers. The MAGFD values related to this scenario are represented in Table 4. It is clear that the proposed controller presents the lowest MAGFD than the other controllers.

5.5. Scenario 5

This scenario evaluates the proposed FOCC performance under a reduction of 50% in the K_{ESS} value to consider more critical conditions. Moreover, severe perturbations, according to Figure 9a–c are also considered as load, solar irradiation, and wind speed, respectively. The system frequency performance for this scenario employing the different controllers is indicated in Figure 9d. As demonstrated, the proposed controller improves the system output from viewpoints of less amplitude oscillations than the other controllers. The MAGFD values of presented controllers related to this scenario are denoted in Table 4. Similar to the prior scenarios, the suggested controller in this scenario also provides the lowest value than the other controllers.

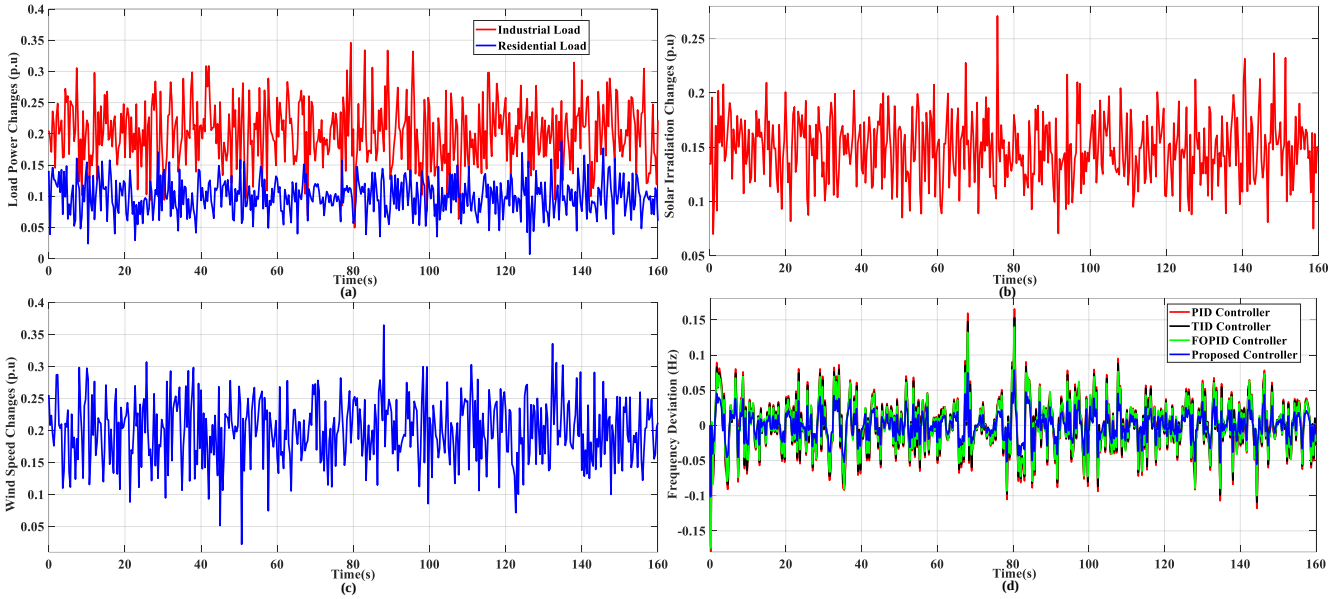

Figure 8. Perturbations and simulation result for scenario 4. (**a**) Load disturbances. (**b**) Wind speed changes. (**c**) Solar irradiation changes. (**d**) Obtained frequency responses.

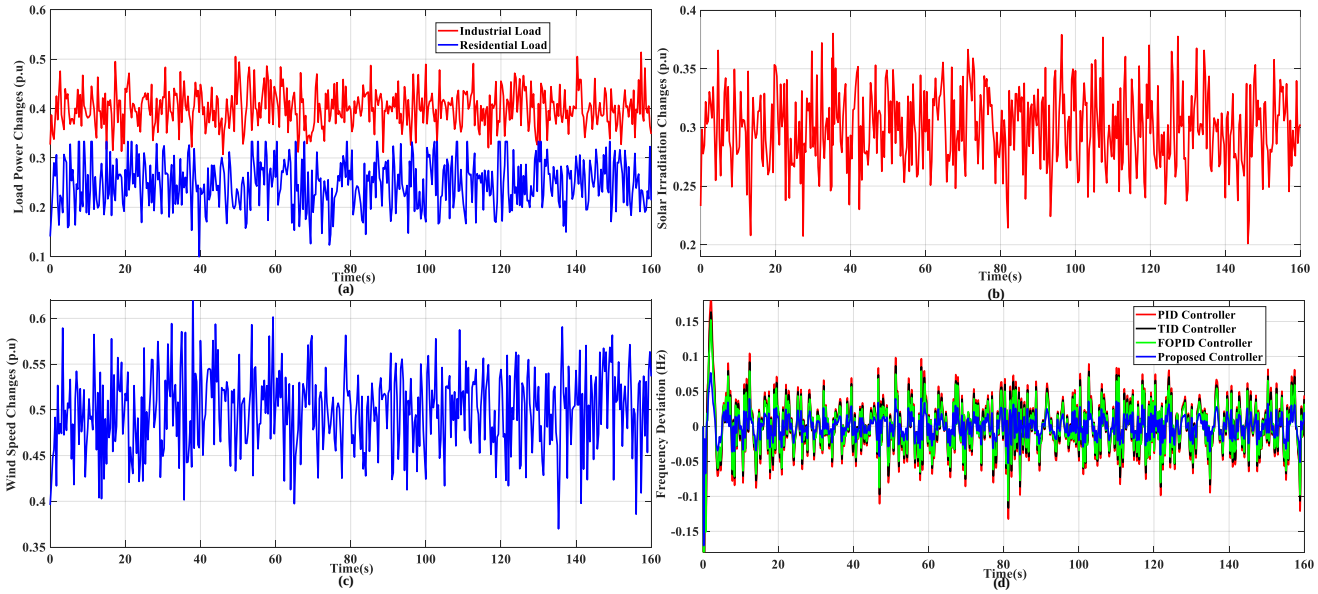

Figure 9. Perturbations and simulation result for scenario 5. (**a**) Load disturbances. (**b**) Wind speed changes. (**c**) Solar irradiation changes. (**d**) Obtained frequency responses.

5.6. Sensitivity Analysis

This subsection analyzes the robustness of the proposed FOCC controller against the system parameters' changes. In this regard, the ±30% variations are applied to T_g and T_t parameters under scenario 1 conditions. Figure 10a,b demonstrates the MG frequency responses attained by the proposed FOCC controller under normal conditions and ±30% reduction in the T_g and T_t parameters, respectively. According to these figures, it can be noted that the responses under normal conditions and considered changes are almost similar. The MAGFD values for this subsection are presented in Table 5. This table reveals that these changes do not significantly impact the MAGFD values using the proposed FOCC controller. Accordingly, the system stays stable.

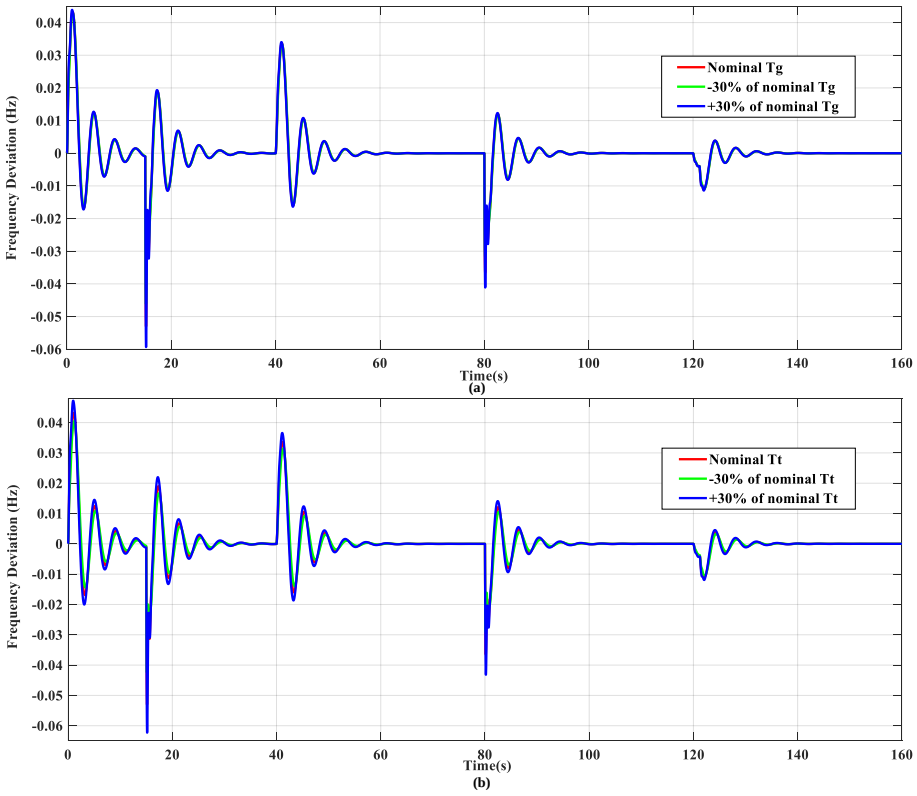

Figure 10. System sensitivity analysis using the presented FOCC controller during ±30% changes in (**a**) T_g (**b**) T_t.

Table 5. Sensitivity analysis for the proposed controller under ±30% changes in Tg and Tt.

Controller	Parameter		MAGFD
Proposed FOCC	T_g	+30%	0.0051
		−30%	0.0045
	T_t	+30%	0.0055
		−30%	0.0043

6. Conclusions

This paper studied the LFC task of an islanded MG in the presence of high participation of RESs. In this regard, an FOCC controller was proposed as the secondary controller to improve the system frequency performance. The proposed FOCC controller has cascaded an FOPI controller with a FOTD controller. An ESS based on the VI control was used to improve the total inertia of the MG. The performance of the suggested FOCC controller was compared with the PID, TID, and FOPID controllers under various perturbations and operating conditions. The tunable parameters of the presented controllers were optimized by the KA method. The results revealed that the presented FOCC controller offers a better frequency response than the other controllers. Eventually, the sensitivity analysis indicated that the suggested FOCC controller is robust versus the coefficients' changes in the system.

Author Contributions: Conceptualization, S.O. and A.F.; methodology, A.O.; software, S.O.; validation, S.O., A.F. and A.O.; formal analysis, M.H.K.; investigation, A.O.; resources, M.H.K.; data curation, A.F.; writing—original draft preparation, S.O.; writing—review and editing, A.F. and A.O.; supervision, M.H.K. All authors have read and agreed to the published version of the manuscript.

Funding: This research received no external funding.

Data Availability Statement: Not applicable.

Conflicts of Interest: The authors declare no conflict of interest.

References

1. Khooban, M.H. An Optimal Non-Integer Model Predictive Virtual Inertia Control in Inverter-Based Modern AC Power Grids-Based V2G Technology. *IEEE Trans. Energy Convers.* **2021**, *36*, 1336–1346. [CrossRef]
2. Zhao, Z.; Guo, J.; Luo, X.; Lai, C.S.; Yang, P.; Lai, L.L.; Li, P.; Guerrero, J.M.; Shahidehpour, M. Distributed Robust Model Predictive Control-Based Energy Management Strategy for Islanded Multi-Microgrids Considering Uncertainty. *IEEE Trans. Smart Grid* **2022**, *13*, 2107–2120. [CrossRef]
3. Bera, A.; Chalamala, B.R.; Byrne, R.H.; Mitra, J. Sizing of Energy Storage for Grid Inertial Support in Presence of Renewable Energy. *IEEE Trans. Power Syst.* **2022**, *37*, 3769–3778. [CrossRef]
4. Fathollahi, A.; Derakhshandeh, S.Y.; Ghiasian, A.; Khooban, M.H. Utilization of dynamic wireless power transfer technology in multi-depot, multi-product delivery supply chain. *Sustain. Energy Grids Netw.* **2022**, *32*, 100836. [CrossRef]
5. Farsizadeh, H.; Gheisarnejad, M.; Mosayebi, M.; Rafiei, M.; Khooban, M.H. An Intelligent and Fast Controller for DC/DC Converter Feeding CPL in a DC Microgrid. *IEEE Trans. Circuits Syst. II Express Briefs* **2020**, *67*, 1104–1108. [CrossRef]
6. Kang, W.; Li, Q.; Gao, M.; Li, X.; Wang, J.; Xu, R.; Chen, M. Distributed secondary control method for islanded microgrids with communication constraints. *IEEE Access* **2017**, *6*, 5812–5821. [CrossRef]
7. Olabi, A.; Abdelkareem, M.A. Renewable energy and climate change. *Renew. Sustain. Energy Rev.* **2022**, *158*, 112111. [CrossRef]
8. Ranjan, M.; Shankar, R. A literature survey on load frequency control considering renewable energy integration in power system: Recent trends and future prospects. *J. Energy Storage* **2022**, *45*, 103717. [CrossRef]
9. Zuo, Y.; Yuan, Z.; Sossan, F.; Zecchino, A.; Cherkaoui, R.; Paolone, M. Performance assessment of grid-forming and grid-following converter-interfaced battery energy storage systems on frequency regulation in low-inertia power grids. *Sustain. Energy Grids Netw.* **2021**, *27*, 100496. [CrossRef]
10. Oshnoei, S.; Aghamohammadi, M.; Oshnoei, S. A Novel Fractional order controller based on Fuzzy Logic for Regulating the Frequency of an Islanded Microgrid. In Proceedings of the 2019 International Power System Conference (PSC), Tehran, Iran, 9–11 December 2019; pp. 320–326.
11. Oshnoei, A.; Kheradmandi, M.; Muyeen, S.M. Robust Control Scheme for Distributed Battery Energy Storage Systems in Load Frequency Control. *IEEE Trans. Power Syst.* **2020**, *35*, 4781–4791. [CrossRef]
12. Kerdphol, T.; Rahman, F.S.; Watanabe, M.; Mitani, Y.; Turschner, D.; Beck, H.-P. Enhanced virtual inertia control based on derivative technique to emulate simultaneous inertia and damping properties for microgrid frequency regulation. *IEEE Access* **2019**, *7*, 14422–14433. [CrossRef]
13. Shahgholian, G.; Mardani, E.; Fattollahi, A. Impact of PSS and STATCOM devices to the dynamic performance of a multi-machine power system. *Eng. Technol. Appl. Sci. Res.* **2017**, *7*, 2113–2117. [CrossRef]
14. Habibi, M.; Oshnoei, A.; Vahidinasab, V.; Oshnoei, S. Allocation and sizing of energy storage system considering wind uncertainty: An approach based on stochastic SCUC. In Proceedings of the 2018 Smart Grid Conference (SGC), Sanandaj, Iran, 28–29 November 2018; pp. 1–6.
15. Khezri, R.; Oshnoei, A.; Oshnoei, S.; Bevrani, H.; Muyeen, S. An intelligent coordinator design for GCSC and AGC in a two-area hybrid power system. *Appl. Soft Comput.* **2019**, *76*, 491–504. [CrossRef]
16. Oshnoei, S.; Oshnoei, A.; Mosallanejad, A.; Haghjoo, F. Novel load frequency control scheme for an interconnected two-area power system including wind turbine generation and redox flow battery. *Int. J. Electr. Power Energy Syst.* **2021**, *130*, 107033. [CrossRef]
17. Fathollahi, A.; Kargar, A.; Derakhshandeh, S.Y. Enhancement of power system transient stability and voltage regulation performance with decentralized synergetic TCSC controller. *Int. J. Electr. Power Energy Syst.* **2022**, *135*, 107533. [CrossRef]
18. Abubakr, H.; Guerrero, J.M.; Vasquez, J.C.; Mohamed, T.H.; Mahmoud, K.; Darwish, M.M.F.; Dahab, Y.A. Adaptive LFC Incorporating Modified Virtual Rotor to Regulate Frequency and Tie-Line Power Flow in Multi-Area Microgrids. *IEEE Access* **2022**, *10*, 33248–33268. [CrossRef]
19. Barbalho, P.I.N.; Lacerda, V.A.; Fernandes, R.A.S.; Coury, D.V. Deep reinforcement learning-based secondary control for microgrids in islanded mode. *Electr. Power Syst. Res.* **2022**, *212*, 108315. [CrossRef]
20. Guerrero, J.M.; Vasquez, J.C.; Matas, J.; De Vicuña, L.G.; Castilla, M. Hierarchical control of droop-controlled AC and DC microgrids—A general approach toward standardization. *IEEE Trans. Ind. Electron.* **2010**, *58*, 158–172. [CrossRef]
21. Oshnoei, S.; Aghamohammadi, M.; Oshnoei, S.; Oshnoei, A.; Mohammadi-Ivatloo, B. Provision of Frequency Stability of an Islanded Microgrid Using a Novel Virtual Inertia Control and a Fractional Order Cascade Controller. *Energies* **2021**, *14*, 4152. [CrossRef]
22. Kanellos, F.D. Real-time control based on multi-agent systems for the operation of large ports as prosumer microgrids. *IEEE Access* **2017**, *5*, 9439–9452. [CrossRef]
23. Fathi, A.; Shafiee, Q.; Bevrani, H. Robust frequency control of microgrids using an extended virtual synchronous generator. *IEEE Trans. Power Syst.* **2018**, *33*, 6289–6297. [CrossRef]

24. Fini, M.H.; Golshan, M.E.H. Determining optimal virtual inertia and frequency control parameters to preserve the frequency stability in islanded microgrids with high penetration of renewables. *Electr. Power Syst. Res.* **2018**, *154*, 13–22. [CrossRef]
25. Kerdphol, T.; Rahman, F.S.; Mitani, Y.; Watanabe, M.; Küfeoğlu, S.K. Robust virtual inertia control of an islanded microgrid considering high penetration of renewable energy. *IEEE Access* **2017**, *6*, 625–636. [CrossRef]
26. Kerdphol, T.; Rahman, F.S.; Watanabe, M.; Mitani, Y. Robust virtual inertia control of a low inertia microgrid considering frequency measurement effects. *IEEE Access* **2019**, *7*, 57550–57560. [CrossRef]
27. Zhang, X.; Zhu, Z.; Fu, Y.; Shen, W. Multi-objective virtual inertia control of renewable power generator for transient stability improvement in interconnected power system. *Int. J. Electr. Power Energy Syst.* **2020**, *117*, 105641. [CrossRef]
28. Ali, H.; Magdy, G.; Li, B.; Shabib, G.; Elbaset, A.A.; Xu, D.; Mitani, Y. A new frequency control strategy in an islanded microgrid using virtual inertia control-based coefficient diagram method. *IEEE Access* **2019**, *7*, 16979–16990. [CrossRef]
29. Abubakr, H.; Vasquez, J.C.; Hassan Mohamed, T.; Guerrero, J.M. The concept of direct adaptive control for improving voltage and frequency regulation loops in several power system applications. *Int. J. Electr. Power Energy Syst.* **2022**, *140*, 108068. [CrossRef]
30. Oshnoei, A.; Khezri, R.; Muyeen, S.; Oshnoei, S.; Blaabjerg, F. Automatic generation control incorporating electric vehicles. *Electr. Power Compon. Syst.* **2019**, *47*, 720–732. [CrossRef]
31. Oshnoei, S.; Oshnoei, A.; Mosallanejad, A.; Haghjoo, F. Contribution of GCSC to regulate the frequency in multi-area power systems considering time delays: A new control outline based on fractional order controllers. *Int. J. Electr. Power Energy Syst.* **2020**, *123*, 106197. [CrossRef]
32. Peddakapu, K.; Srinivasarao, P.; Mohamed, M.R.; Arya, Y.; Krishna Kishore, D.J. Stabilization of frequency in Multi-Microgrid system using barnacle mating Optimizer-based cascade controllers. *Sustain. Energy Technol. Assess.* **2022**, *54*, 102823. [CrossRef]
33. Singh, K.; Arya, Y. Tidal turbine support in microgrid frequency regulation through novel cascade Fuzzy-FOPID droop in de-loaded region. *ISA Trans.* **2022**, *133*, 218–232. [CrossRef] [PubMed]
34. Dash, P.; Saikia, L.C.; Sinha, N. Automatic generation control of multi area thermal system using Bat algorithm optimized PD–PID cascade controller. *Int. J. Electr. Power Energy Syst.* **2015**, *68*, 364–372. [CrossRef]
35. Aziz, S.; Wang, H.; Liu, Y.; Peng, J.; Jiang, H. Variable universe fuzzy logic-based hybrid LFC control with real-time implementation. *IEEE Access* **2019**, *7*, 25535–25546. [CrossRef]
36. Pothiya, S.; Ngamroo, I. Optimal fuzzy logic-based PID controller for load–frequency control including superconducting magnetic energy storage units. *Energy Convers. Manag.* **2008**, *49*, 2833–2838. [CrossRef]
37. Tian, E.; Peng, C. Memory-based event-triggering H∞ load frequency control for power systems under deception attacks. *IEEE Trans. Cybern.* **2020**, *50*, 4610–4618. [CrossRef]
38. Pandey, S.K.; Mohanty, S.R.; Kishor, N.; Catalão, J.P. Frequency regulation in hybrid power systems using particle swarm optimization and linear matrix inequalities based robust controller design. *Int. J. Electr. Power Energy Syst.* **2014**, *63*, 887–900. [CrossRef]
39. Sun, W.; Fang, Z.; Huang, L.; Li, Q.; Li, W.; Xu, X. Distributed robust secondary control of islanded microgrid with stochastic time-varying delays and external disturbances. *Int. J. Electr. Power Energy Syst.* **2022**, *143*, 108448. [CrossRef]
40. Mohanty, B.; Hota, P.K. Comparative performance analysis of fruit fly optimisation algorithm for multi-area multi-source automatic generation control under deregulated environment. *IET Gener. Transm. Distrib.* **2015**, *9*, 1845–1855. [CrossRef]
41. Khalili, J.; Dehkordi, N.M.; Hamzeh, M. Distributed event-triggered secondary frequency control of islanded AC microgrids under cyber attacks with input time delay. *Int. J. Electr. Power Energy Syst.* **2022**, *143*, 108506. [CrossRef]
42. Chamorro, H.R.; Riaño, I.; Gerndt, R.; Zelinka, I.; Gonzalez-Longatt, F.; Sood, V.K. Synthetic inertia control based on fuzzy adaptive differential evolution. *Int. J. Electr. Power Energy Syst.* **2019**, *105*, 803–813. [CrossRef]
43. Veerasamy, V.; Wahab, N.I.A.; Ramachandran, R.; Othman, M.L.; Hizam, H.; Irudayaraj, A.X.R.; Guerrero, J.M.; Kumar, J.S. A Hankel matrix based reduced order model for stability analysis of hybrid power system using PSO-GSA optimized cascade PI-PD controller for automatic load frequency control. *IEEE Access* **2020**, *8*, 71422–71446. [CrossRef]
44. Smith, E.J.; Robinson, D.A.; Agalgaonkar, A.P. A secondary strategy for unbalance consensus in an islanded voltage source converter-based microgrid using cooperative gain control. *Electr. Power Syst. Res.* **2022**, *210*, 108097. [CrossRef]
45. Daraz, A.; Malik, S.A.; Azar, A.T.; Aslam, S.; Alkhalifah, T.; Alturise, F. Optimized Fractional Order Integral-Tilt Derivative Controller for Frequency Regulation of Interconnected Diverse Renewable Energy Resources. *IEEE Access* **2022**, *10*, 43514–43527. [CrossRef]
46. Tripathi, S.; Singh, V.P.; Kishor, N.; Pandey, A. Load frequency control of power system considering electric Vehicles' aggregator with communication delay. *Int. J. Electr. Power Energy Syst.* **2023**, *145*, 108697. [CrossRef]
47. Zaid, S.A.; Bakeer, A.; Magdy, G.; Albalawi, H.; Kassem, A.M.; El-Shimy, M.E.; AbdelMeguid, H.; Manqarah, B. A New Intelligent Fractional-Order Load Frequency Control for Interconnected Modern Power Systems with Virtual Inertia Control. *Fractal Fract.* **2023**, *7*, 62. [CrossRef]
48. Bahrampour, E.; Dehghani, M.; Asemani, M.H.; Abolpour, R. Load frequency fractional-order controller design for shipboard microgrids using direct search alghorithm. *IET Renew. Power Gener.* **2023**, *17*, 894–906. [CrossRef]
49. Yin, L.; Cao, X.; Chen, L. High-dimensional Multiple Fractional Order Controller for Automatic Generation Control and Automatic Voltage Regulation. *Int. J. Control Autom. Syst.* **2022**, *20*, 3979–3995. [CrossRef]
50. Sahoo, G.; Sahu, R.K.; Samal, N.R.; Panda, S. Analysis of type-2 fuzzy fractional-order PD-PI controller for frequency stabilisation of the micro-grid system with real-time simulation. *Int. J. Sustain. Energy* **2022**, *41*, 412–433. [CrossRef]

51. Kumar, A.; Pan, S. Design of fractional order PID controller for load frequency control system with communication delay. *ISA Trans.* **2022**, *129*, 138–149. [CrossRef]
52. Warrier, P.; Shah, P. Fractional order control of power electronic converters in industrial drives and renewable energy systems: A review. *IEEE Access* **2021**, *9*, 58982–59009. [CrossRef]
53. Tepljakov, A.; Alagoz, B.B.; Yeroglu, C.; Gonzalez, E.A.; Hosseinnia, S.H.; Petlenkov, E.; Ates, A.; Cech, M. Towards industrialization of FOPID controllers: A survey on milestones of fractional-order control and pathways for future developments. *IEEE Access* **2021**, *9*, 21016–21042. [CrossRef]
54. Muresan, C.I.; Birs, I.; Ionescu, C.; Dulf, E.H.; De Keyser, R. A review of recent developments in autotuning methods for fractional-order controllers. *Fractal Fract.* **2022**, *6*, 37. [CrossRef]
55. Podlubny, I. *Chapter 10—Survey of Applications of the Fractional Calculus*; Fractional Differential Equations; Elsevier: Amsterdam, The Netherlands, 1999; Volume 198.
56. Aboelela, M.A.; Hennas, R.H.M. Development of a Fractional-Order PID Controller Using Adaptive Weighted PSO and Genetic Algorithms with Applications. In *Fractional Order Systems*; Elsevier: Amsterdam, The Netherlands, 2018; pp. 511–551.
57. Thakar, U.; Joshi, V.; Mehta, U.; Vyawahare, V.A. Fractional-order PI controller for permanent magnet synchronous motor: A design-based comparative study. In *Fractional Order Systems*; Elsevier: Amsterdam, The Netherlands, 2018; pp. 553–578.
58. Shahgholian, G.; Fattollahi, A. Improving power system stability using transfer function: A comparative analysis. *Eng. Technol. Appl. Sci. Res.* **2017**, *7*, 1946–1952. [CrossRef]
59. Hall, J.E. *Pocket Companion to Guyton & Hall Textbook of Medical Physiology E-Book*; Elsevier Health Sciences: Amsterdam, The Netherlands, 2015.
60. Ekinci, S.; Demiroren, A.; Hekimoglu, B. Parameter optimization of power system stabilizers via kidney-inspired algorithm. *Trans. Inst. Meas. Control* **2019**, *41*, 1405–1417. [CrossRef]
61. Jaddi, N.S.; Alvankarian, J.; Abdullah, S. Kidney-inspired algorithm for optimization problems. *Commun. Nonlinear Sci. Numer. Simul.* **2017**, *42*, 358–369. [CrossRef]
62. Idir, A.; Kidouche, M.; Bensafia, Y.; Khettab, K.; Tadjer, S.A. Speed control of DC motor using PID and FOPID controllers based on differential evolution and PSO. *Int. J. Intell. Eng. Syst* **2018**, *20*, 21. [CrossRef]
63. Shabani, H.; Vahidi, B.; Ebrahimpour, M. A robust PID controller based on imperialist competitive algorithm for load-frequency control of power systems. *ISA Trans.* **2013**, *52*, 88–95. [CrossRef]
64. Bruni, R.; Celani, F. Combining global and local strategies to optimize parameters in magnetic spacecraft control via attitude feedback. *J. Optim. Theory Appl.* **2019**, *181*, 997–1014. [CrossRef]